A PARAMETRIC STUDY OF DIMENSIONAL TOLERANCE AND HYDRODYNAMIC DEBRIS REMOVAL IN MICRO-ELECTRO-DISCHARGE MACHINING

Mark T. Richardson[1*], Yogesh B. Gianchandani[1], and Dawn S. Skala[2]
[1]*Department of Electrical Engineering and Computer Science, University of Michigan, Ann Arbor*
[2]*Microprocessing Department, Sandia National Laboratories, Livermore, CA*

ABSTRACT

This paper reports a detailed evaluation of batch mode micro-electro-discharge machining (μEDM) of 316L stainless steel. Lithographically fabricated copper tools with parallel line features of 5-50 μm width and 5-75 μm spacing were used to quantify trends in machining tolerance and the impact of debris accumulation. As tool feature density increased, debris accumulation effects began to dominate, eventually destroying both tool and workpiece. A two-step hydrodynamic debris removal technique yielded significant improvements in surface and edge finish, machining time, and tool wear over past work using standard vertical dither flushing.

I. INTRODUCTION

Micro-electro-discharge machining (μEDM) utilizes controlled spark discharges between a tool and workpiece that are both immersed in dielectric oil. Any electrically conductive material can be machined and is useful in the micro-fabrication of devices from cardiac stents to relays [1-2]. Serial mode μEDM, which is relatively understood [3], utilizes a sharpened wire tip as the tool. However, batch mode μEDM, which uses lithographically patterned tools (e.g. LIGA electroplated Cu) is 100x faster [4] but has some open questions.

Self-created machining debris are critical in determining tolerances for both serial mode and batch mode EDM [5]. In serial mode, the machining tool can be both rotated and vertically dithered to flush out debris. However, in batch mode, the tool movement is limited to the dither motion. Further, the large planar extent of the tool and its high-aspect ratio features limit options for flushing.

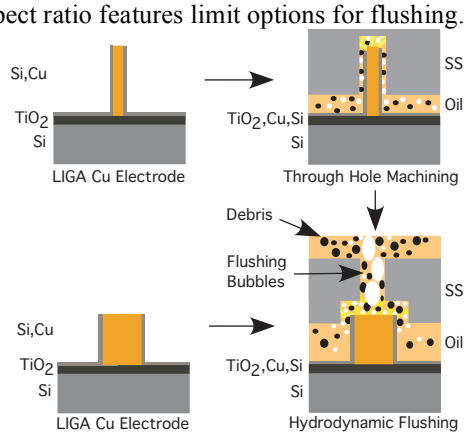

Fig. 1: Machining process for debris flushing. Step 1: machine narrow through-holes, Step 2: machine finished pattern overlaid on top. Flushing bubbles and tool dither force debris out the through-hole.

The resulting accumulation of debris can cause workpiece surface damage and excessive tool wear due to spurious discharges. The problem is exacerbated as feature density increases. Eventually, debris accumulation between the tool and the workpiece causes uncontrolled arcing. High temperatures cause the tool to melt and recast into a mushroom shape, limiting both vertical cutting depth and lateral resolution. Passivating the sidewalls of the tool with thin film coatings improves tool wear and workpiece roughness for low aspect ratio structures [6], but machining significantly slows for high aspect ratio structures. The coating is only a partial solution since it is eventually destroyed by discharges in high densities of debris. A two-step hydrodynamic debris removal technique (Fig. 1) yielded significant improvements in surface and edge finish, machining time, and tool wear over past work using standard vertical dither flushing.

Section II describes the design and fabrication of the tools and experiments; section III presents a hydraulic resistance model for debris flushing; and section IV presents the experimental results.

II. DESIGN AND FABRICATION

Three types of test patterns were selected to represent different microenvironments:

1. Parallel Trench

The dimensional tolerance of batch μEDM features was evaluated using 600 μm long parallel trenches machined by four parallel lines of 5-50 μm width and 5-75 μm spacing (Table I). The layout allowed for machining of 16 different sets of features at once while minimizing debris movement among different features. Machining parameters for this experiment are given in Table I and were chosen for optimal surface roughness and edge finish at the expense of machining time.

2. Enclosed Perimeter

Four large holes within an enclosed perimeter represent structures with large machining fill-factors. These patterns are resistant to flushing by the normal vertical tool dither in dielectric oil (Table II). In these types of patterns, debris generated by μEDM accumulates within the perimeter and forms conductive paths to the workpiece, causing machining to self-terminate. The plated Cu tool was coated with 200 nm of sputtered Si for this study and the following study to suppress lateral discharges at low levels of debris. Silicon was chosen because it is resistive enough to prevent spark discharges on the sidewalls during normal machining, it is still conductive enough to discharge at the tip when desired,

*Corresponding Author: 1301 Beal, Ann Arbor, MI 48109. mtrichar@umich.edu

and it can be deposited with a lithographically compatible sputtering process [6].

3. Hydrodynamic Debris Removal

The enclosed perimeter pattern was also evaluated with a new two-step machining method that facilitates hydrodynamic removal of debris. By first µEDM-machining narrow through-holes in the workpiece, a path is created for the debris to escape when the pattern is machined (Fig. 1). Locating these through-holes in the field region of the final die does not disrupt the pattern. In this study the through-holes were formed by 60 µm X 60 µm posts located on the tool die next to the actual pattern (Fig. 3). Thus, the workpiece was machined sequentially by two different parts of the tool die in separate steps.

4. Copper Tool Fabrication

Copper tools ranging from 175-200 µm tall were fabricated by Sandia National Laboratories CA using PMMA LIGA on a low-Z titanium oxide seed layer. These tools were used to machine patterns part way into 100 µm 316L stainless steel workpieces – the kind used for commercial stents. The workpiece was mounted to an aluminum mandrel using silver epoxy. Care was taken to prevent bending the workpiece since 316L stainless steel is relatively soft.

III. DEBRIS FLUSHING MODELING

The performance of the hydrodynamic debris removal technique cannot be directly modeled readily since it is a

Table I: Dimensional variation and machining conditions for parametric study.

Parametric Dimensional Study	
Tool Height	200µm, 175µm
Feature Length	600µm
Feature Width	5,10,15,25,50µm
Feature Spacing	5,10,15,18, 20,25,50,75µm
Voltage	70V
Capacitor	10pF
Resistor	5kΩ
Z-Feed	0.2µm/s
Plunge Depth	35µm

Table II: Debris study conditions.

Debris Study	
Tool Height	175µm
Finish Hole	120x120µm
Wall Thickness	40µm
Wall Spacing	120µm
Voltage	70V
Capacitor	10pF
Resistor	5kΩ
Z-Feed	0.2µm/s
Plunge	41, 80µm

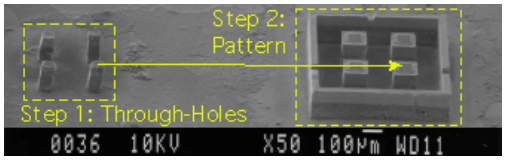

Fig. 3: Hydrodynamic debris flushing test pattern post machining (pattern 3). Through-holes at left while walled finishing structure at right.

complex three-phase flow with changing boundary conditions. Gas and debris particulate generation occurs at unknown rates. Massive temperature and pressure fluctuations result from the spark discharges. The vertical dither of the tool also complicates the model. The standard debris removal mechanism involves fluid flow from the vertical tool dither and gas bubble entrainment. These effects are difficult to quantify by observation. However, by assuming laminar flow, we can compare the hydraulic resistance at the locations of debris generation for a single point in time to gain some qualitative insight on the removal rates of the standard mechanism and the hydrodynamic mechanism.

For laminar flow, the hydraulic resistance of a rectangular channel is given by:

$$R = \frac{12\eta L}{H^3 W - \frac{192}{\pi^5} H^4 \sum_{m=0}^{\infty} (2m+1)^{-5} \tanh\left[\frac{(2m+1)\pi W}{2H}\right]} \quad (1)$$

where η, L, H, W are viscosity, length, height, and width respectively. For a preliminary comparison it is sufficient to examine the relative impact on an equivalent uniaxial hydraulic resistance. A cross section of the hydraulic circuit for the enclosed perimeter is shown in Fig. 4. The point of

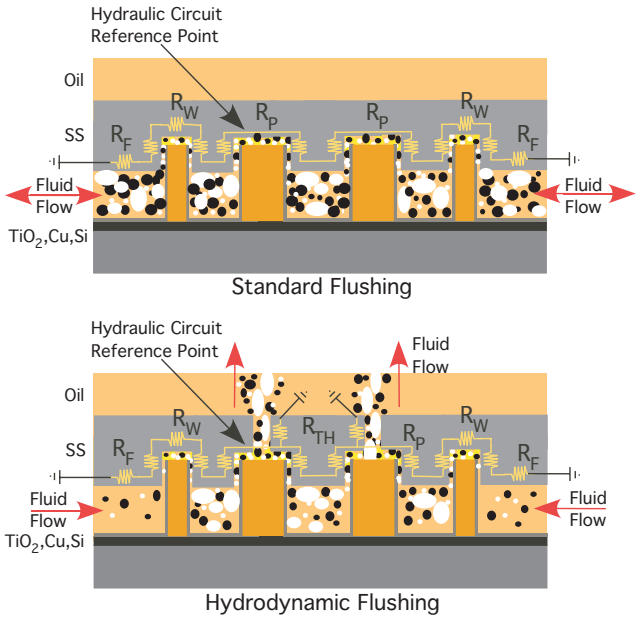

Fig. 4: Cross section of hydraulic resistance circuit for standard dither flushing (top) and hydrodynamic flushing (bottom). Through-holes provide a shunt path for debris to escape by bubble elutriation.

reference for the model is at an inner post with plunge depth of 40 µm and a discharge gap (channel height H) of 6 µm. To simplify the calculation for R_{Wall}, the outer wall can be represented as a rectangle of width W and flow channel length L. Here, W is the perimeter of the feature whereas

$$L = 2*(plunge\_depth) + wall\_width$$

A similar technique is used for R_{Post} and R_{Field}. Since the area of the workpiece is much larger than the machined feature, a channel length of 2 mm is assumed for R_{Field}. The total hydraulic resistance for the standard flushing method is then:

$$R_{ST} = R_{Post} + R_{Wall} + R_{Field} \quad (2)$$

The total hydraulic resistance for hydrodynamic flushing is:

$$R_{HY} = (R_{Post} + R_{Wall} + R_{Field}) // R_{TH1} // (R_{TH2-4} + 2*R_{Post}) \quad (3)$$

Where R_{TH1-4} represent the four through-hole fluidic channels. Using the dimensions stated in Table II and using m=1-10^5, the resistances were found in Matlab to be: R_{Post}=6.96x10^{12}, R_{Wall}=4.39x10^{12}, R_{Field}=6.50x10^9, and R_{TH}=2.31x10^{11} Pa/m^{3}s. This gives R_{ST}=1.14x10^{13} and R_{HY}=2.16x10^{11}, a 53x reduction in steady state hydraulic resistance.

IV. EXPERIMENTAL RESULTS

1. Dimensional Tolerance

Optical imaging was used to measure the width of the tool and workpiece features and compared with a known reference before and after machining. Figure 5 shows the machining tolerance between the machined width and the tool spacing as obtained by test pattern 1. Data points in Fig. 5 and Fig. 7 represent the average of 3 measurements. Three tool feature spacings are shown for clarity in Fig. 5 but there are more complex trends that could not be shown because of paper length considerations. While 5 µm wide features can be machined, it is notable that the tolerances are 5-17 µm, and have a non-linear trend. As can be seen in Fig. 6, debris accumulation and tool recasting play roles in determining tool feature dimensions after machining.

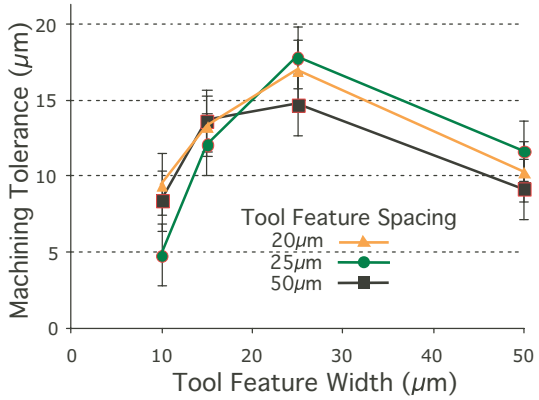

Fig. 5: Machining tolerance, (original tool feature spacing – machined width), shows a non-linear dependence on tool feature width and ranges from 5-17 µm.

One consideration that should be taken into account is that the debris generation rate of a particular tool feature width may not scale at the same rate as the hydraulic resistance R_{Post} modeled in the previous section. For narrow tool features, the debris generation rate is low and the features are easily flushed when reasonably spaced (Fig. 6A). As tool feature width increases, more debris are generated and the machined width increases (Fig 6D, Fig. 5). If the debris removal rate does not scale at the same pace, the debris cannot exit the discharge gap in time to avoid spurious discharges from the sides of the tool features. At sufficiently large tool feature widths, the trend reverses. Large width tool features should be more resilient to recasting since they are able to conduct heat more efficiently than narrow features but there may be other trends at play.

Figure 7 characterizes how the tool feature itself can wear due to lateral discharges or increase due to mushroom-shaped recasting. As the spacing between these features is decreases, debris accumulation makes tool wear very erratic as can be seen in Fig. 6 C,D.

2. Debris Flushing

The enclosed perimeter patterns were machined into the workpiece as deep as possible. The standard flushing pattern self terminated at 41.3 µm due to debris

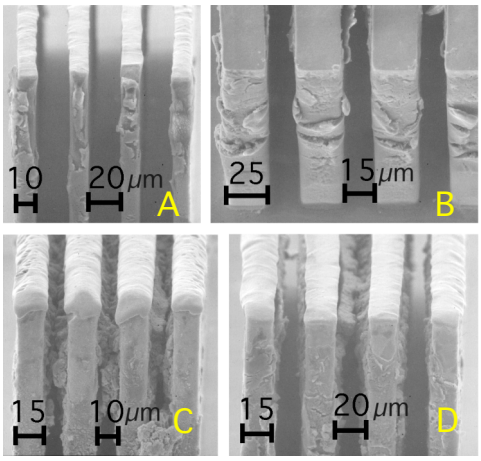

Fig. 6: Copper tool features of various widths and spacing after machining. A and B have little debris and wear. C and D have significant debris and some tool feature recasting.

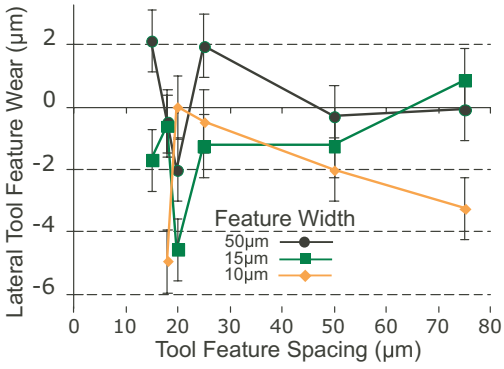

Fig 7: As tool feature spacing reduces, lateral tool feature wear becomes erratic. Tool features widen because debris accumulation causes recasting.

accumulation. The hydrodynamic pattern plunged 125 µm for the through-holes and then 80 µm for the walled structure before being stopped manually. During the second step, the bubbles generated during machining coagulated almost exclusively within the wall perimeter. As the bubbles rose up the through-holes they entrained debris particles (Fig. 8) flushed them out. Bubble size is important because in fluidization column systems, the larger the gas bubbles, the more efficient the solid particle removal [6].

SEM images of the machined workpiece and tools show that the two-step procedure had a dramatic impact on dimensional tolerance, sidewall angle, surface finish, and device height (Fig. 9). These findings create the possibility of high precision machining by batch µEDM.

Figure 10 plots the plunge depth over time for the two flushing methods. Despite machining twice as deep, the two-step flushing method progressed much faster. According to the model in section III, the hydrodynamic hydraulic resistance R_{HY} decreases with increasing depth while the standard flushing resistance R_{ST} increases with increasing depth. The standard method follows a 3rd power trend while the two-step hydrodynamic method follows a linear trend for both steps.

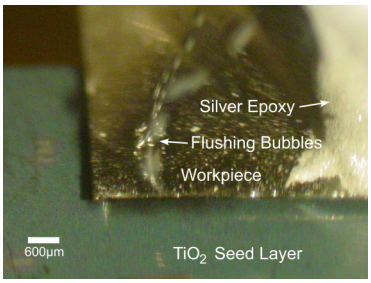

Fig. 8: Hydrodynamic debris flushing through workpiece utilizing bubbles from discharge and vertical dither of tool.

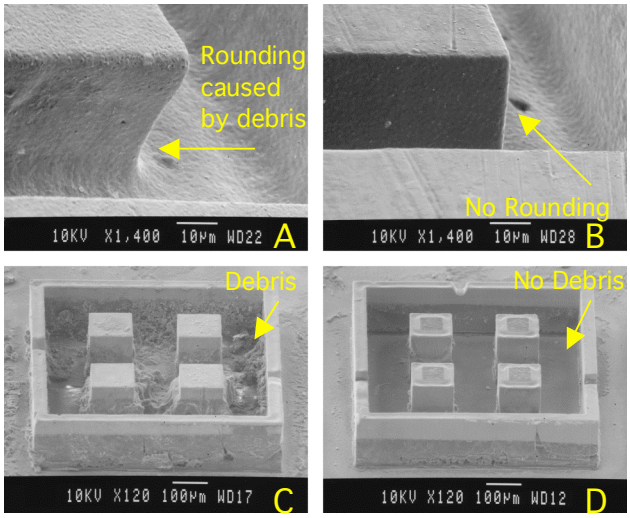

Fig. 9a-d: Enclosed workpiece (41 µm deep, 1h43m) (A) with no flushing. Rough surface on top and sidewalls, angled corner edge. Flushing workpiece (80 µm deep, 1h59m) (B) shows clean sidewall and top surface, sharp corner. Grain structure is still visible on top surface. Enclosed tool feature after machining (C) has a lot of residual debris while flushing tool feature (D) does not. Both utilized Si coated sidewalls.

V. CONCLUSION

A parametric study of dimensional tolerance for batch mode µEDM has been presented. It was found that 10 µm lines required the lowest machining tolerance to produce a desired pattern with a tradeoff on tool wear. Machining tolerance follows a non-linear trend for tool feature spacing and is also affected by debris accumulation. A hydrodynamic flushing method utilizing self generated bubbles for debris entrainment was investigated. A rough estimate obtained using a static uniaxial hydraulic resistance model predicted a 53x reduction by using the new method. Significant improvements in surface and edge finish as well as machining time and depth were observed.

ACKNOWLEDGEMENTS

The authors acknowledge Weibin Zhu, Amar Basu, and Brandon Levey for fabrication assistance as well as Joseph Giachino and Tim Hubbard for dicing. The Advanced Light Source is supported by the Materials Sciences Division, of the U.S. Dept. of Energy under Contract No. DE-AC03-76SF00098 at Lawrence Berkeley National Laboratory. Sandia is operated by Sandia Corp., a Lockheed Martin Company, for the Dept. of Energy's National Nuclear Security Admin. under Contract DE-AC04-94AL85000.

REFERENCES

[1] K. Takahata, A. DeHennis, K.D. Wise, Y.B. Gianchandani, "Stentenna: A Micromachined Antenna Stent for Wireless Monitoring of Implantable Microsensors," *IEEE Conf. EMBS*, 2003, pp. 3360-3.

[2] K. Udeshi, M. Richardson, J.-J. Hung, L. Que, G.M. Rebeiz, Y.B. Gianchandani, "A dual-EDM reverse damascene process for RF switches and other bulk devices," *ASME IMECE*, Nov. 2005, in press.

[3] T. Masaki, K. Kawata, and T. Masuzawa, "Micro Electro-Discharge Machining and Its Applications," *IEEE MEMS '90*, pp. 21-26,1990.

[4] K. Takahata and Y.B. Gianchandani, "Batch Mode Micro-Electro-Discharge Machining," *IEEE J.MEMS* 11(2), pp. 102-110, 2002.

[5] J. McGeough, *Advanced Methods of Machining*. London; New York: Chapman and Hall, pp. 129-151,1988.

[6] M.T. Richardson and Y.B. Gianchandani, "A Passivated Electrode Batch µEDM Technology for Bulk Metal Transducers and Packages," *IEEE Sensors*, November 2005, to be published.

[7] S.H. Yeo and L.K. Tan, "Effects of ultrasonic vibrations in micro-electro-discharge machining of microholes," *IOP J. Micromech. Microeng.*,Vol 9, pp. 345-352, 1999.

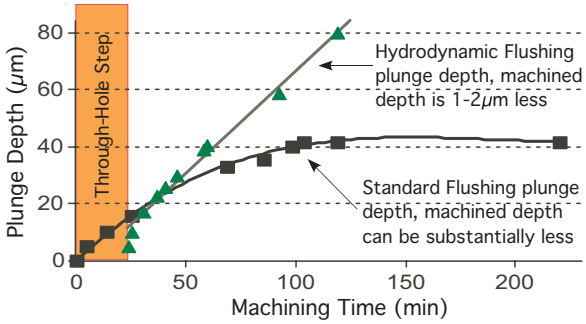

Fig. 10: Standard walled pattern self terminates at 40 µm. Two-step process is faster and a linear trend for each step.